

Influence of Deposition Potential on Electrodeposited Bismuth–Copper Oxide Electrodes for Asymmetric Supercapacitor

Rushikesh G. Bobade,^[a] Niteen B. Dabke,^[b] Shoyebmohamad F. Shaikh,^[c] Abdullah M. Al-Enizi,^[c] Bidhan Pandit,*^[d] Balkrishna J. Lokhande,^[e] and Revanappa C. Ambare*^[a]

The modern research reported the simplest low-cost synthesis of Bismuth–Copper oxide (Bi_2CuO_4) with spruce-leaf-like morphology and its applications in supercapacitor devices. $\text{Bi}(\text{NO}_3)_3 \cdot 5\text{H}_2\text{O}$ was used as a precursor during an electrodeposition (ED) method to create the spruce-leaf-like Bi_2CuO_4 electrode. XRD, XPS, FE-SEM, EDX, and TEM were used to characterize the structures and morphologies of the synthesized materials, while CV, CP, and EIS were used to determine their electrochemical characteristics. The Bi_2CuO_4 phase was con-

firmed by XRD patterns, and electrochemical testing demonstrated that the material had better rate capability and an SC of 431.2 F/g at a scan rate of 2 mV/s. After 5,000 cycles, it retained 81.4% of its energy. Additionally, the maximum SC that was attained by the created asymmetric solid-state device ASSD ($\text{Bi}_{0.6}\text{I}_1$ M PVA-KOHIIAC) was 73.7 F/g. The energy density was 55.3 Wh/Kg at a power density of 4570 W/Kg. The exceptional electrochemical performance of Bi_2CuO_4 thin film electrodes recommends it has a promising material.

Introduction

Supercapacitors, a type of energy storage technology, are gaining prominence for a variety of applications, including electric and hybrid vehicles, gadgets, and energy systems, due to their quick charging–discharging time, high power density, outstanding stability at low temperatures, low operating cost, and environmentally friendly nature.^[1,2,3] They can be separated into two main classes based on their electrical charge-storing

mechanisms: first is electrical double-layer capacitors (EDLC), which have a double-layer charging process, and pseudocapacitors, which store charge by a faradaic reaction. When compared to an EDLC, pseudocapacitors often have a higher energy density. Since RuO_2 shows a high specific capacitance of roughly 720 F/g, it is used as the active material in several transition metal oxide pseudocapacitors.^[4,5] They are dangerous and expensive, however, which restricts their utility. Thin film electrode materials with outstanding electrochemical performance and a cheap cost are thus especially suitable for pseudocapacitors.

Because of its significant band gaps, which result in outstanding photocatalytic performance,^[6] excessive refractive index, photoluminescence, remarkable photoconductivity, and dielectric permittivity,^[7] Bi_2O_3 is a significant semiconductor material. Applications that are widely used, like gas sensors,^[8] optical materials,^[9] fuel cells,^[10] and solar cells,^[11] are particularly suitable due to these features. Numerous Bi_2O_3 micro- and nanostructures, such as nanofibers,^[12] nanobelts,^[13] nanoflakes,^[14] nanowires,^[15] nano-flowers,^[16] particles,^[17] and thin films^[18] have been successfully synthesized. Generally, Bi_2O_3 has five leading polymorphic arrangements, known as, $\alpha\text{-Bi}_2\text{O}_3$ (monoclinic), $\beta\text{-Bi}_2\text{O}_3$ (tetragonal), $\gamma\text{-Bi}_2\text{O}_3$ (BCC), $\delta\text{-Bi}_2\text{O}_3$ (cubic), and $\omega\text{-Bi}_2\text{O}_3$ (triclinic). The monoclinic and cubic forms of $\alpha\text{-Bi}_2\text{O}_3$ at moderate low and high temperatures, respectively, are generally stable phases, whereas the other forms are metastable.^[19]

Nanocrystalline Bi_2O_3 features include a large surface area, well-defined electrolytic redox exertion, and pseudo-capacitive behavior, which are the components of supercapacitors.^[20] There are limited reports about the creation of Bi_2O_3 material-based electrodes. Y. W. Park *et al.*^[14] fabricated graphene-bismuth oxide using the facile solvothermal method. The

[a] R. G. Bobade, R. C. Ambare

Department of Physics, KMC, College, Khopoli, Khopoli-410203 (Affiliated to University of Mumbai), M.S. India
E-mail: revanambare@gmail.com

[b] N. B. Dabke

Central Analytical Facility, CSIR-National Chemical Laboratory, Dr. Homi Bhabha Road, Pune- 411008, India

[c] S. F. Shaikh, A. M. Al-Enizi

Department of Chemistry, College of Science, King Saud University, P.O. Box 2455, Riyadh 11451, Saudi Arabia

[d] Dr. B. Pandit

Department of Materials Science and Engineering and Chemical Engineering, Universidad Carlos III de Madrid, Avenida de la Universidad 30, 28911 Leganés, Madrid, Spain
E-mail: bpandit@ing.uc3m.es
physics.bidhan@gmail.com

[e] B. J. Lokhande

Lab of Electrochemical Studies, School of Physical Sciences, PSAH Solapur University, Solapur, Maharashtra, India

 Supporting information for this article is available on the WWW under <https://doi.org/10.1002/batt.202400163>

 © 2024 The Authors. Batteries & Supercaps published by Wiley-VCH GmbH. This is an open access article under the terms of the Creative Commons Attribution Non-Commercial NoDerivs License, which permits use and distribution in any medium, provided the original work is properly cited, the use is non-commercial and no modifications or adaptations are made.

FE-SEM image showed nanoflake-like morphology. They stated a maximum SC of 757 F/g at 10 A/g. R. Chen *et al.*^[15] synthesized CNT@Bi₂O₃ via the hydrothermal method with nanowire-like morphology. The reported highest SE was 98.2 Wh/kg at SP of 48.1 Kw/Kg with 80% of the maximum capacity over 8000 cycles. H. Xu *et al.*^[16] fabricated Bi₂O₃ via the electro-spinning method. It showed a maximum SC of 786.2 mF/g in 1 M Na₂SO₄. They reported the maximum energy density and power density was 11.3 Wh/kg and 3.37 Kw/kg respectively. Hong Su *et al.*^[21] synthesized rod-like Bi₂O₃ electrode. Its maximum SC was 1350 F/g at 0.1 A/g of current density. N. Xia *et al.*^[22] successfully synthesized bismuth oxide on mesoporous carbon. The calculated highest SC was 386 F/g.

The current work describes a simple and highly efficient approach for the ED synthesis of compounds containing bismuth oxide on copper substrates. It is a simple process that, without the use of a template, may result in excellent crystalline grade, nanometre-sized, and uniform particles. Because of its simple composition mechanism, low treating temperature, and advantageous electrochemical characteristics, the electrodeposition process is a desirable technique.^[23] Additionally, the formation processes and electrochemical characteristics of the produced Bi₂CuO₄, such as CV, CP, and EIS, were examined.

Experimental Section

Growth of Bismuth Dioxide on Copper Substrate

A copper substrate with a surface area of 1.5×5 cm² was chosen as the substrate for bismuth dioxide deposition. The copper substrate was first ultrasonically cleaned with 10% HCl for 5 minutes to eliminate any probable contaminants before being rinsed for 1 minute with acetone and double-distilled water (DDW). In a typical three-electrode electrochemical setup, platinum wire (Pt) was used as the counter electrode and was electrodeposited in an aqueous barium nitrate solution with a constant concentration of 0.0125 M. The foamed thin film electrode served as the working electrode, while the Ag/AgCl was used as the reference electrode. At different deposition potentials of 0.4 V, 0.5 V, and 0.6 V, 15 minutes of bismuth oxide depositions on the copper substrate were conducted and they were nominated as Bi_{0.4}V, Bi_{0.5}V, and Bi_{0.6}V electrodes. All electrodes were annealed at 573 K for 60 minutes before being utilized for electrochemical, morphological, and structural analyses. Figure S1 shows the design for the three-electrode deposition of bismuth oxide on a conducting copper substrate electrode.^[24]

Synthesis of Activated Carbon Electrode

Polyvinyl alcohol (PVA) of 1 gm and DDW of 10 ml were combined to create a PVA solution, which was then stirred at 80° to 90°C for 2 to 3 hours. Activated carbon (AC) and PVA solution were then combined for 2 hours at 80°–90°C. Using a desiccator, the created PVA–AC solution was dried. The generated uniform slurry was cast onto the cleaned copper substrate. The thin film was created by flattening a slurry with a doctor blade that was 20–30 cm in size and 200–350 mm thick. The electrode was initially dried for 4 hours at ambient temperature before being tempered in a muffle furnace for 6–7 hours at 353 K.^[25]

Synthesis of PVA–KOH

4 gm of KOH and 3 gm of PVA were used to make the alkaline gel polymer electrolyte, which was used as a separator. To create a clear, viscous solution, 3 gm of PVA was first dissolved in 60 ml of DDW and vigorously stirred at 85° to 90°C. When the solution had gradually cooled to room temperature, 4 gm of KOH was added, and stirring was maintained for 5–6 hours at that temperature. The electrolyte separator, constructed of alkaline gel polymer, was used to make an asymmetric solid-state device (ASSD) by pouring the clear adhesive solution into a petri dish and letting it air dry at room temperature.^[26]

Fabrication of Asymmetric Solid-State Supercapacitor

It was possible to build an asymmetric solid-state supercapacitor (Bi_{0.6}V||1 M PVA–KOH||AC) device to investigate the real-world applications of the created materials. This assembly used 1 M PVA–KOH as the separator–electrolyte to separate the positive bismuth–cobalt–copper oxide thin film electrode from the negative optimized activated carbon electrode.^[26]

Characterization Details

A Rigaku D/max 2550 Vb⁺/PC 18 kW with Cu K α =1.5406 diffractometer was used to assess the crystal structure, plane orientations, and phase purity. A Hitachi S-4800, 15 kV field emission scanning electron microscope (FE-SEM) was used to produce the energy-dispersive X-ray spectroscopy (EDX) and microstructure images. The contact angle of the constructed electrode was measured using the Holmark HO-IAD-CAN-01 equipment. Using a 1×10⁻⁶ high-precision analytical microbalance (Tapson's-100 TS), the weight difference technique was used to calculate the weight of the depositing substance. X-ray photoelectron spectroscopy (XPS) analysis was carried out using a Thermo ESCALab 250Xi spectrometer with an Al K α (1486.7 eV) monochromatic radiation source. The photoluminescence (PL) spectrum at an emission wavelength of 365 nm was analyzed using a Horiba Fluorog-2 Jobnyvon spectrometer. A computer-controlled potentiostat (HCH 600D SPL. electrochemical analyzer/workstation) was used to investigate the electrochemical parameters of three electrode cells of a Bi₂CuO₄ film electrode. Throughout the cyclic voltammetry (CV) of the produced electrodes (size 1.5 cm²) in 1 M KOH, saturated Ag/AgCl was used as the reference electrode, and platinum wire functioned as the counter electrode in the supercapacitive investigation. The SC was calculated using relation 1 and the obtained from CV curves. At varying current densities, the specific energy (SE) and specific power (SP) of charge–discharge were studied using chronopotentiometry (CP). The internal resistance of a supercapacitor cell was evaluated using a multi-frequency electrochemical impedance frequency (EIS) test with an AC signal ranging from 1 mHz to 1 MHz.

Electrochemical Measurements

The electrochemical characteristics of individual electrodes and the ASSD device were assessed using the HCH 600D SPL electrochemical workstation. A standard three-electrode setup was used, consisting of the reference electrode made of (Ag/AgCl), the counter electrode made of platinum (Pt) wire, and working electrodes i.e. Bi₂CuO₄ composite in a 1 M KOH. The electrochemical performances of the as-obtained electrodes were studied using GCD and CV plots. The electrochemical impedance spectroscopy analyses were attempted at 10 mV AC amplitude and in the frequency range of 100 Hz to 1 MHz. From CV curves, SC values in

F/g were estimated. The SE in Wh/kg, and SP in kW/kg, were obtained using GCD plots and the following relations.^[23,24]

$$SC = \frac{1}{mv(V_c - V_a)} \int_{V_a}^{V_c} I(V)dV \quad (1)$$

$$SE = \frac{V \times I_d \times t_d}{m} \quad (2)$$

$$SP = \frac{V \times I_d}{m} \quad (3)$$

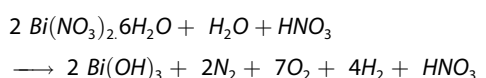
Where, 'V' is the scan rate, '(V_c–V_a)' it's a potential window, 'I (V)' its current, m its active mass on electrode material, 'V' its voltage, 'I_d' its discharged current, 't_c' its charging time, and 't_d' its discharging time.

Results and Discussion

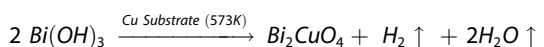
Bi₂CuO₄ Film Formation Kinetics

Bi (NO₃)₃ aqueous solutions were electrolyzed at molar concentrations of 0.0125 M for 15 minutes, resulting in the production of a bismuth hydroxide coating on the working electrode by evolving H₂ gas. In the electrodeposition procedures, hydrogen bubbles accompanied a reduction of H⁺ ions at cathodic overpotential, which was the reason.^[27] On a copper substrate, hydroxyl ions from water molecules interacted with Bi³⁺ ions to generate the Bi(OH)₃ film.

Bismuth oxide deposited on copper substrate

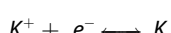
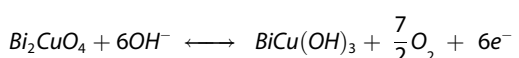


Finally obtained black colour film of Bi(OH)₃ annealed at 573 K for 60 min.



Obtained bismuth oxide film on a copper substrate in yellowish colour.

During an electrolysis



During the process of electrochemical evaluation, O₂ gas is produced and the oxi-hydroxide phase containing bismuth-copper oxide gets formed.

Structural and XPS Analysis

The XRD patterns of the produced Bi₂CuO₄ samples are shown in Figure 1 (a). The major peaks at 28.4°, 32.1°, 33.1°, 43.8°, 46.5°, 51.0°, 55.8°, and 74.6° were assigned to the diffractions of the (220), (012), (130), (222), (411), (421), (332), and (314) planes of the tetragonal phase Bi₂CuO₄, which was in excellent agreement with Match Entry No. 96–100–6029. Figure S2 illustrates the observed and baseline XRD results were in agreement. A slow XRD scan was used to measure the crystallite size (d) for samples Bi_{0.4}V, Bi_{0.5}V, and Bi_{0.6}V samples. The computed average grain size values were 37.4 nm, 35.5 nm, and 32.8 nm, respectively, using Scherer's relation.^[28] It was discovered that as the deposition potential rose, peak intensity increased and average crystalline grain size decreased, going from 37.4 to 32.8 nm. It was notable that the detected peaks are intense and well-defined, indicating that the samples were well-crystallized in their prepared state. The micro-strain was calculated using the following equation.^[23]

$$\epsilon = \frac{\beta}{4\tan\theta} \quad (4)$$

The determined micro-strain values for the Bi_{0.4}V, Bi_{0.5}V, and Bi_{0.6}V films were 0.031, 0.035, and 0.037, respectively. The Bi_{0.4}V electrode exhibited low microstrain, indicating that the Bi_{0.4}V layer was usually well-ordered with few lattice distortions. However, the Bi_{0.5}V electrode showed that its lattice characteristics may have deviated slightly from Bi_{0.4}V, causing lattice strain and distortions and resulting in a larger micro-strain value than the Bi_{0.4}V electrode. The Bi_{0.6}V electrode demonstrated that incorporating Bi_{0.5}V into the Bi_{0.4}V lattice resulted in bigger lattice distortions and a higher micro-strain value than Bi_{0.4}V or Bi_{0.5}V thin films.

XPS analysis was utilized to investigate the composition of the components and the chemical oxidation of the parts present in the manufactured materials, as shown in Figure 1(b-f). The elements Bi, Cu, O, and C were found in the sample Bi_{0.6}V composite, according to the XPS whole survey scan spectrum shown in Figure 1 (b), similar results reported by P. J. Mafa *et al.*^[29] With two separate peaks of Bi 4f with horizontal separations of 5.27 eV at 158.8 eV and 164.1 eV for Bi₂CuO₄ shows in Figure 1 (c). These peaks were caused by doublet spin-orbital photoelectron emission from the Bi 4f_{7/2} and Bi 4f_{5/2} states. Figure 1 (d) showed a high-precision XPS of Cu 2p in Bi₂CuO₄. It revealed two distinct peaks with a horizontal separation of 19.87 eV, actual peaks at 933.17 eV and 953.28 eV, which were related to photoelectron emission from the Cu 2p_{3/2} and Cu 2p_{1/2} microstates, respectively. Due to the varied chemical environments and interactions with other components, these main peaks had been lowered back to the binding energy in the sample Bi_{0.6}V combination. This occurrence indicated how Bi₂CuO₄ may have operated as an electron receiver, allowing electrons to go to the material and change the electron density around Cu⁺. Similar outcomes were shown by P. J. Mafa *et al.*^[29] Furthermore, the Cu 2p spectrum of Bi₂CuO₄ exhibited satellite peaks at 941.3 eV, 943.5 eV, and 962.4 eV. These satellite peaks confirmed the existence of divalent copper in the materials.^[29]

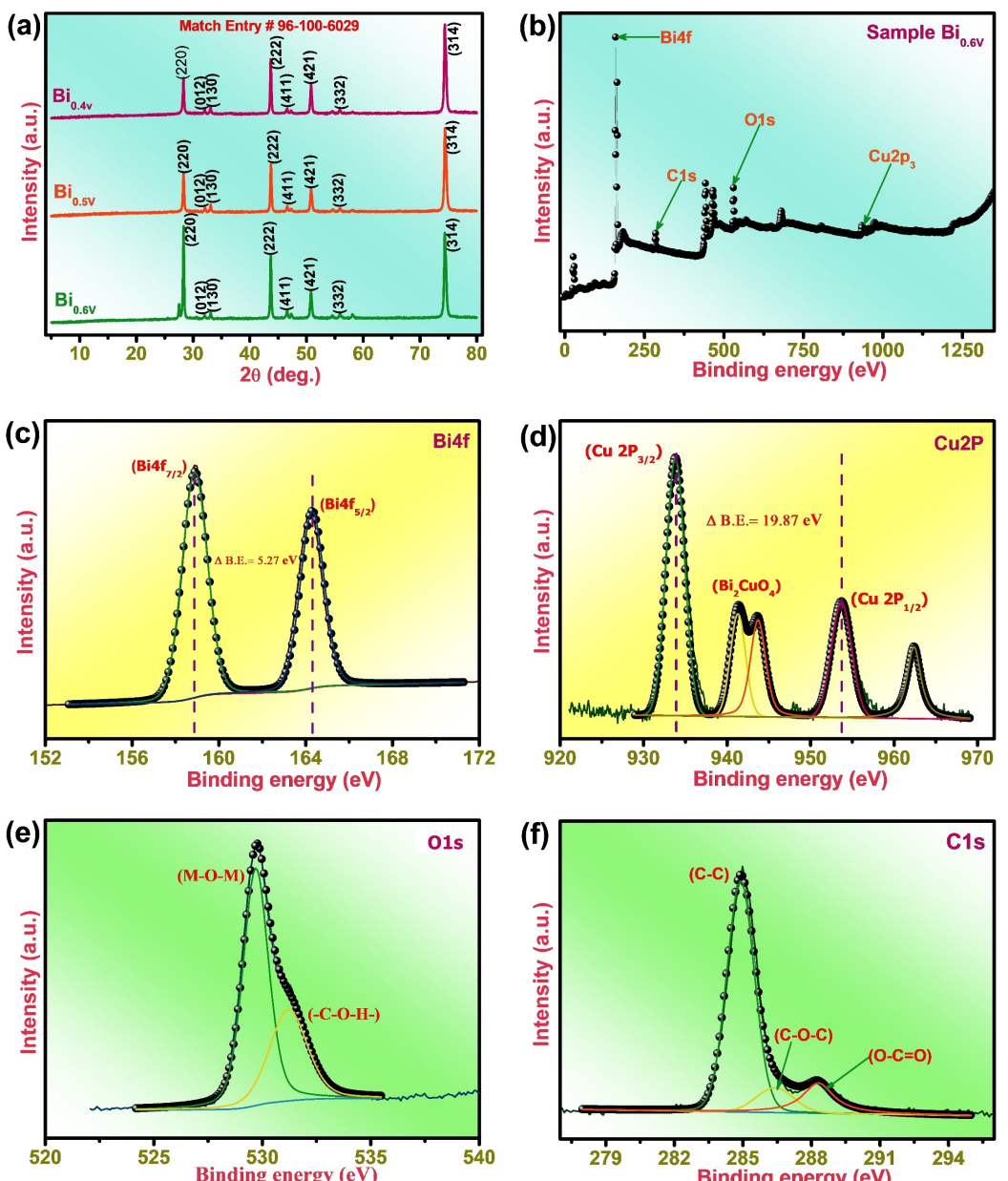


Figure 1. (a) XRD patterns of sample $\text{Bi}_{0.4\text{V}}$, $\text{Bi}_{0.5\text{V}}$, & $\text{Bi}_{0.6\text{V}}$, (b) full range survey XPS spectrum of sample $\text{Bi}_{0.6\text{V}}$; and enlarged spectra (c) of $\text{Bi}4\text{f}$, and (d) $\text{Cu}2\text{p}$, (e) $\text{O}1\text{s}$, (f) $\text{C}1\text{s}$.

Figure 1 (e) showed two photoelectron peaks in the $\text{O}1\text{s}$ detailed spectra. The oxygen in the metal–oxygen–metal ($\text{M}-\text{O}-\text{M}$) connection that was part of the spinel structural lattice caused the peak at 529.1 eV. Peaks at 531.8 eV showed the existence of $(-\text{C}-\text{O}-\text{H}-)$. The above-mentioned carbon bonds could have provided a platform for rapid electron transit, resulting in high conductivity for the material. Interactions between the oxygen-containing functional groups on the copper substrate and the nanoparticles (NPs) via covalent chemical bonds, static attraction, or van der Waal's forces may also have increased hybrid material resolution.^[30] Figure 1 (f) shown the combinations high-resolution $\text{C}1\text{s}$ spectra, which revealed the carbon–carbon single bond $\text{C}-\text{C}$ peak at 284.4 eV, the $\text{C}-\text{O}-\text{C}$ peak at 286.3 eV, and the $\text{O}-\text{C}=\text{O}$ peak at 288.2 eV.^[30]

Morphological Analysis

The FE-SEM images of Bi_2CuO_4 nanoparticles with various deposition potentials was revealed in Figure 2. Figure 2 (a–f) shows the FE-SEM images of sample $\text{Bi}_{0.4\text{V}}$, $\text{Bi}_{0.5\text{V}}$, and $\text{Bi}_{0.6\text{V}}$ at various magnifications ranging from $3\text{ }\mu\text{m}$ to 300 nm . All FE-SEM images had an architecture resembling a spruce leaf, similar results were described by Ahmed AL-Osta *et al.*^[31] For $\text{Bi}_{0.4\text{V}}$, $\text{Bi}_{0.5\text{V}}$, and $\text{Bi}_{0.6\text{V}}$, the particle sizes were determined to be 35.9 nm, 34.1 nm, and 31.2 nm, respectively. This conclusively demonstrates that the particle size reduces as the deposition potential was rising. The wettability images of samples $\text{Bi}_{0.4\text{V}}$, $\text{Bi}_{0.5\text{V}}$, and $\text{Bi}_{0.6\text{V}}$ were displayed in Figure S3 (a–c), respectively. The contact angles for samples $\text{Bi}_{0.4\text{V}}$, $\text{Bi}_{0.5\text{V}}$, and $\text{Bi}_{0.6\text{V}}$ were discovered to be 84.4, 46.0, and 20.4,

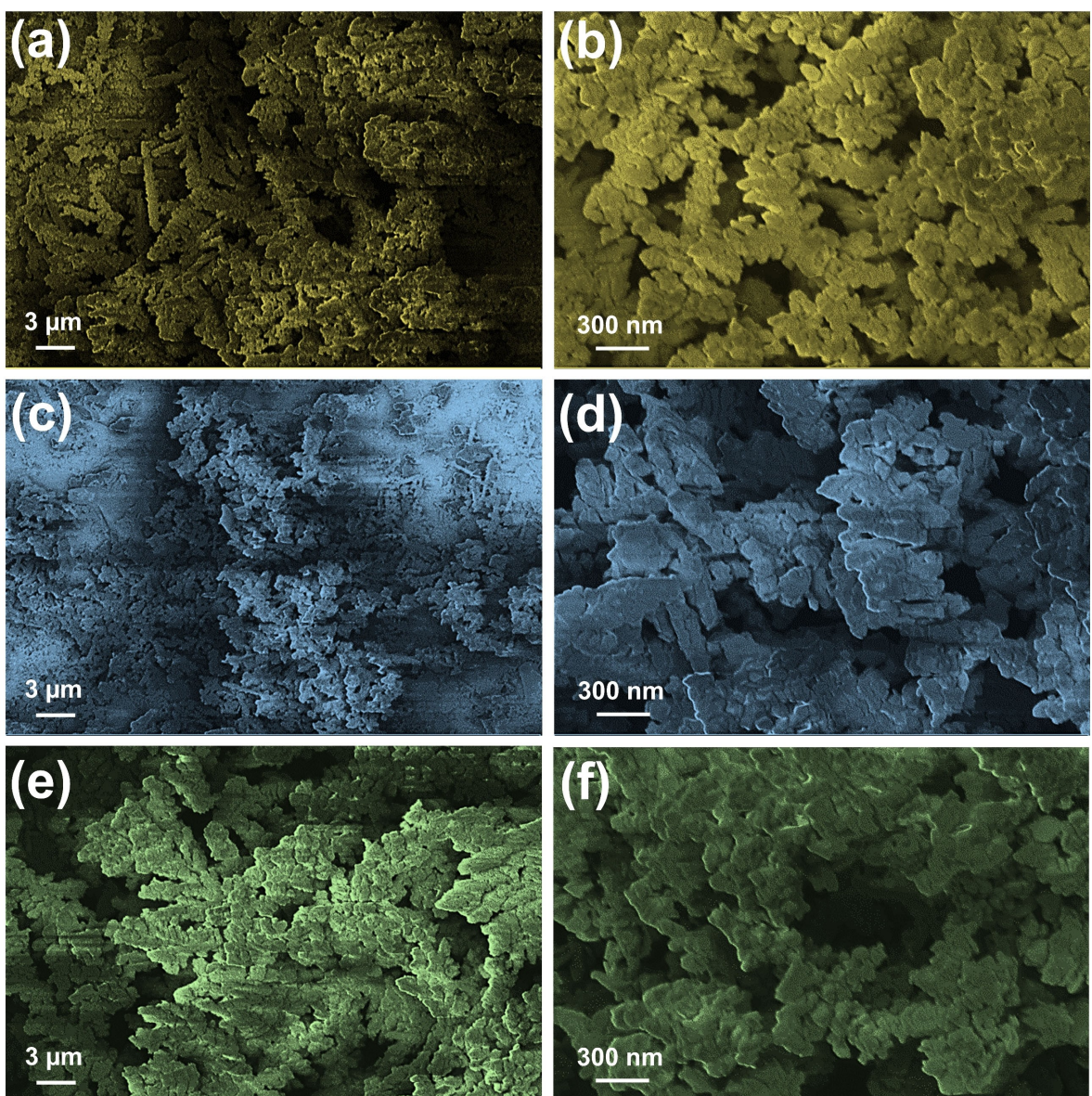


Figure 2. FE-SEM image at 3 μm scale of sample (a) $\text{Bi}_{0.4\text{V}}$, (c) $\text{Bi}_{0.5\text{V}}$, (e) $\text{Bi}_{0.6\text{V}}$; High magnification FE-SEM images at 300 nm of the sample (b) $\text{Bi}_{0.4\text{V}}$, (d) $\text{Bi}_{0.5\text{V}}$, (f) $\text{Bi}_{0.6\text{V}}$.

respectively. All samples of the wettability study demonstrate the hydrophilic nature of the material. From these images, it is clear that with increasing deposition potential, the contact angle decreases.

Figure 3 (a-d) shows the elemental mapping of Bi, Cu, and O, respectively. All three elements (Bi, Cu, and O) are present and distributed homogeneously, according to the elemental mappings. It should be noted that the Bi, Cu, and O concentrations are shown, suggesting that the produced sample was made of Bi_2CuO_4 . Figure 3 (e) displays the EDX spectra graph of sample $\text{Bi}_{0.6\text{V}}$. Bismuth, copper, and oxygen peaks are present. The TEM images of the $\text{Bi}_{0.6\text{V}}$ electrode (Bi_2CuO_4) are revealed in Figure 3 (f & g). It displayed a plaque-like (flake) structure, which is consistent with the results obtainable by S. Anandana *et al.*^[32] The cause for this assembled structure might be due to joining components comprised of edge-

sharing CuO_n units prescribed in planar groups; in other words, copper ions in Bi_2CuO_4 were synchronizing by square oxygen ion planes, which were then combined above one another in a staggered way to form 1D copper ion chains.^[32]

Supercapacitor Performance

The cyclic voltammetry (CV) plot of three separate electrodes $\text{Bi}_{0.4\text{V}}$, $\text{Bi}_{0.5\text{V}}$, and $\text{Bi}_{0.6\text{V}}$ at a scan rate of 2 mV/s was revealed in Figure 4 (a). The CV curve exhibits good symmetry, indicating that the material has suitable reversibility. As can be observed, the CV curve of electrode $\text{Bi}_{0.6\text{V}}$ had the biggest closed area because bismuth-copper oxide deposits more quickly at higher voltages. Figure 4 (b) shows the CV curves of electrode $\text{Bi}_{0.6\text{V}}$ at different scan rates from

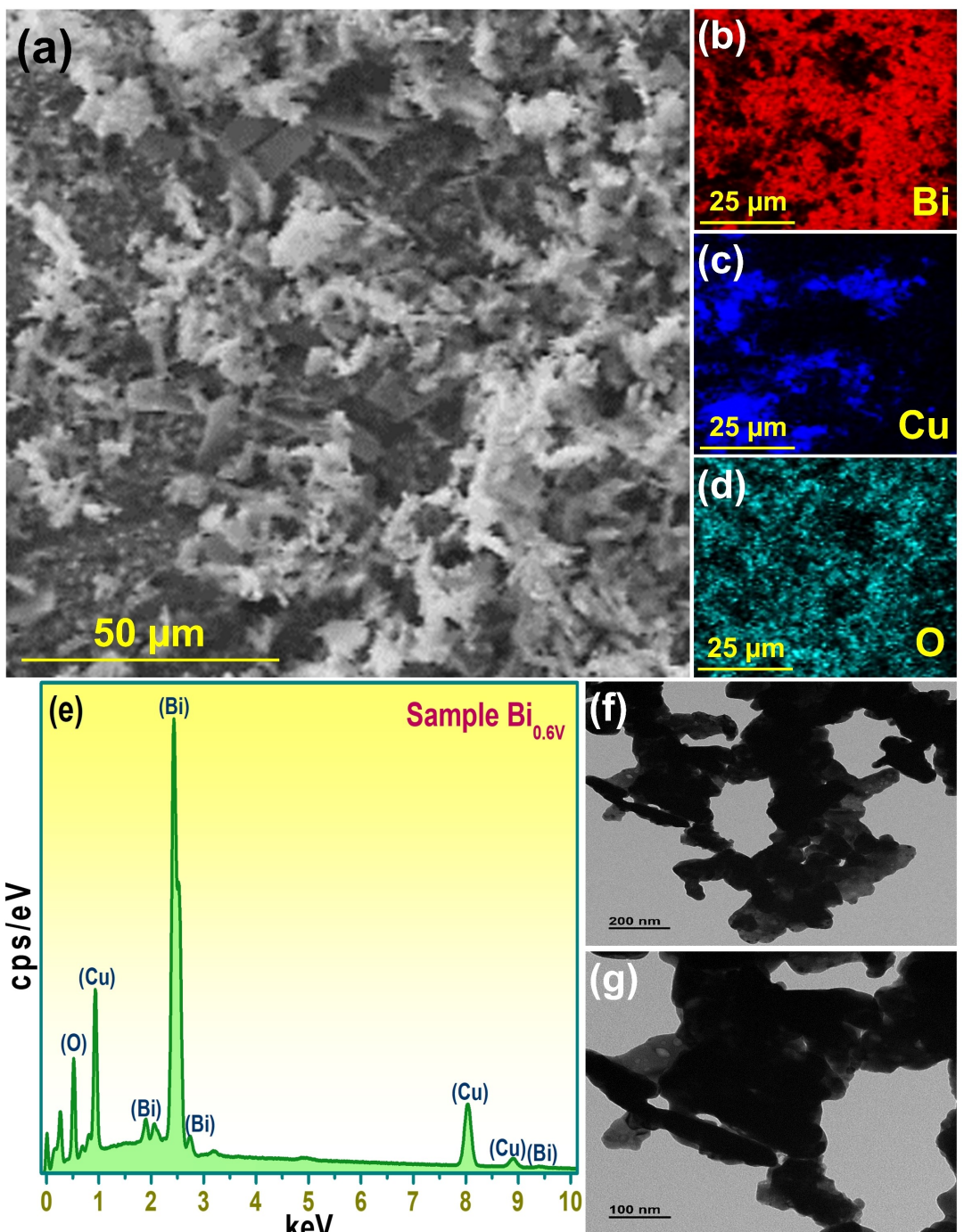


Figure 3. (a-d) EDS elemental mapping analysis of sample $\text{Bi}_{0.6V}$, (e) EDX spectrum images of sample $\text{Bi}_{0.6V}$, (f) TEM images of sample $\text{Bi}_{0.6V}$ at 200 nm, (g) High resolution TEM image of sample $\text{Bi}_{0.6V}$ at 100 nm.

2 to 100 mV/s. Mixed capacitive behavior was confirmed by all CV curves. As shown in Figure 4 (c), the electrode $\text{Bi}_{0.6V}$ calculates values of 431.2, 424.4, 395.6, 321.5, and 164.6 F/g SC at 2, 5, 10, 20, 50, and 100 mV/s, respectively. Table 1 compares the electrochemical properties of bismuth oxide with those of other bismuth oxides in aqueous electrolytes that have been reported. Regarding the effectiveness of the supercapacitor thin film electrode, electrochemical redox activity was crucial for enhancing the pseudo-faradaic surface redox reactions utilizing the electrolyte, and the

ionic size of the electrolyte was crucial for ionic conductivity and ionic intercalation. The Bi_2CuO_4 matrix was easily intercalated by electrolytic K^+ ions, improving the electrochemical performance. Additionally, it should be observed that the oxidation and reduction peaks, respectively, partially moved in more positive and negative orientations. Even at a scan rate of 100 mV/s, the redox peaks were still clearly visible, demonstrating that the electrode $\text{Bi}_{0.6V}$ had a strong rate capacity even at a higher scan rate. Peak shifting was not as distinct, indicating that the electrode was highly reversible at

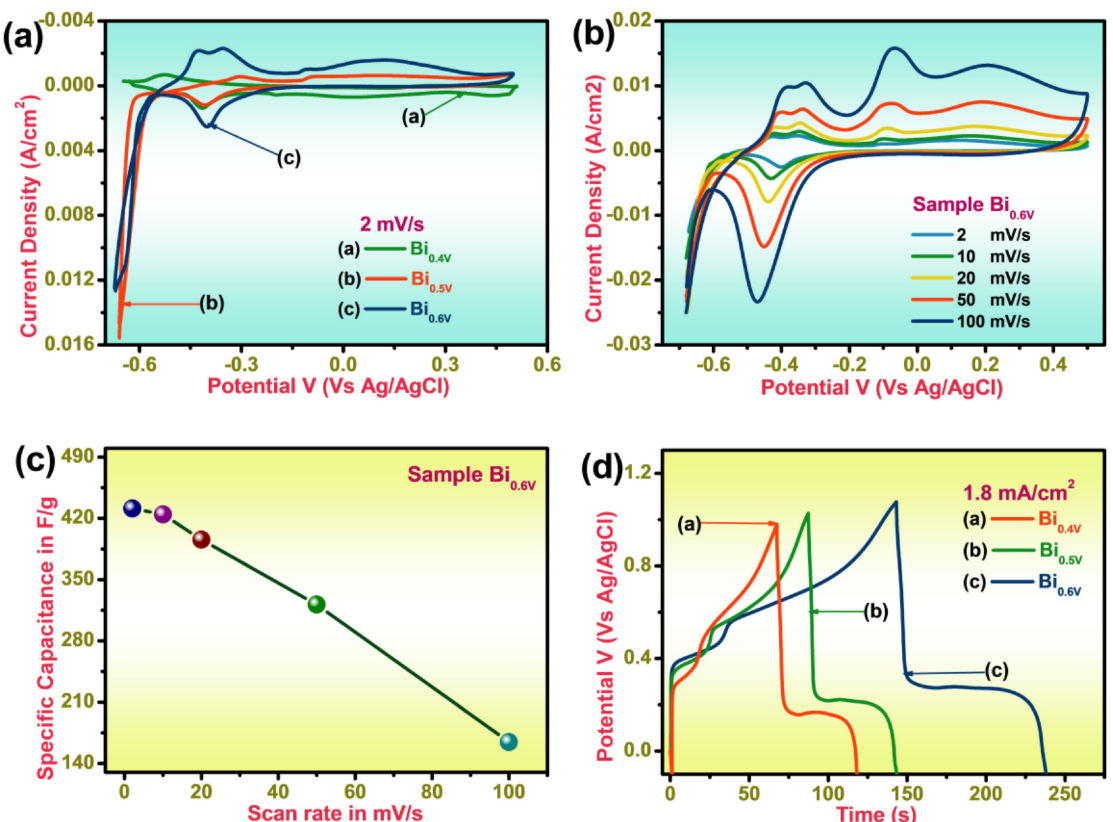


Figure 4. Electrochemical characterization of the Bi₂CuO₄ thin film electrode; (a) CV curve of Bi₂CuO₄ for as prepared Bi_{0.4V}, Bi_{0.5V}, & Bi_{0.6V} electrode annealed at 573 K scanned in 1 M KOH electrolyte at 2 mV/s, (b) Bi_{0.6V} electrode at various scan rates from 2 to 100 mV/s, (c) specific capacitance in F/g of Bi_{0.6V} electrode at different scan rate, (d) chronopotentiometry curve of electrode Bi_{0.4V}, Bi_{0.5V} & Bi_{0.6V} in 1 M KOH at 1.8 mA/cm² current density.

maximum scan rates. The electrochemical efficiency of the electrode Bi_{0.6V} was evaluated using the Chronopotentiometry (CP) technique. When scanned in 1 M KOH at 1.8 mA/cm², Figure 4 (d) showed the charging–discharging behavior of Bi₂CuO₄ formed on a conducting copper substrate with different applied potentials Bi_{0.4V}, Bi_{0.5V}, and Bi_{0.6V}. All CP curves showed an IR drop, and the charging curve showed a little rise before declining with extended plateaus. This was the beauty of bismuth oxide, as confirmed by the fact that its

discharge signatures differed from those of other materials. The polarization effect may have been impacted by a system's irreversibility.^[23,28]

The chronopotentiometry technique is used to examine the CP behavior of the Simple Bi_{0.6V} (Bi₂CuO₄) electrode at 1.0, 1.2, 1.4, 1.6, and 1.8 mA/cm² current densities at 1.19 V operating voltage shown in Figure 5 (a). The charging–discharging time reduces with increasing current density, indicating a tendency towards linear

Table 1. Comparison of electrochemical characteristics of Bi₂CuO₄ with other reported bismuth oxide in aqueous electrolyte.

Sr. No.	Electrode	Synthesis Method	Electrolyte	SC in F/g	SE in Wh/kg	SP in kW/Kg	Stability			Ref.
							Retention (%)	Cycles	Ref.	
1.	Graphene–bismuth oxide	Facile solvothermal	–	757	–	–	65	1000	14	
2.	CNT@Bi ₂ O ₃	Hydrothermal	6 M KOH	–	98.2	48.1	80	8000	15	
3.	Bi ₂ O ₃	Electrospinning technology	1 M Na ₂ SO ₄	786.2 mF/g	11.3	3.37	87	2000	16	
4.	Bi ₂ O ₃	Precipitation method	–	1350	–	–	2.4	1,000	21	
5.	carbon@Bi ₂ O ₃	Hydrothermal	6 M KOH	386	–	–	2.0	1,000	22	
6.	Bi ₂ CuO ₄	Electrodeposition	1 M KOH	431.2	82.7	350 W/Kg	81.4	5000	In this work	

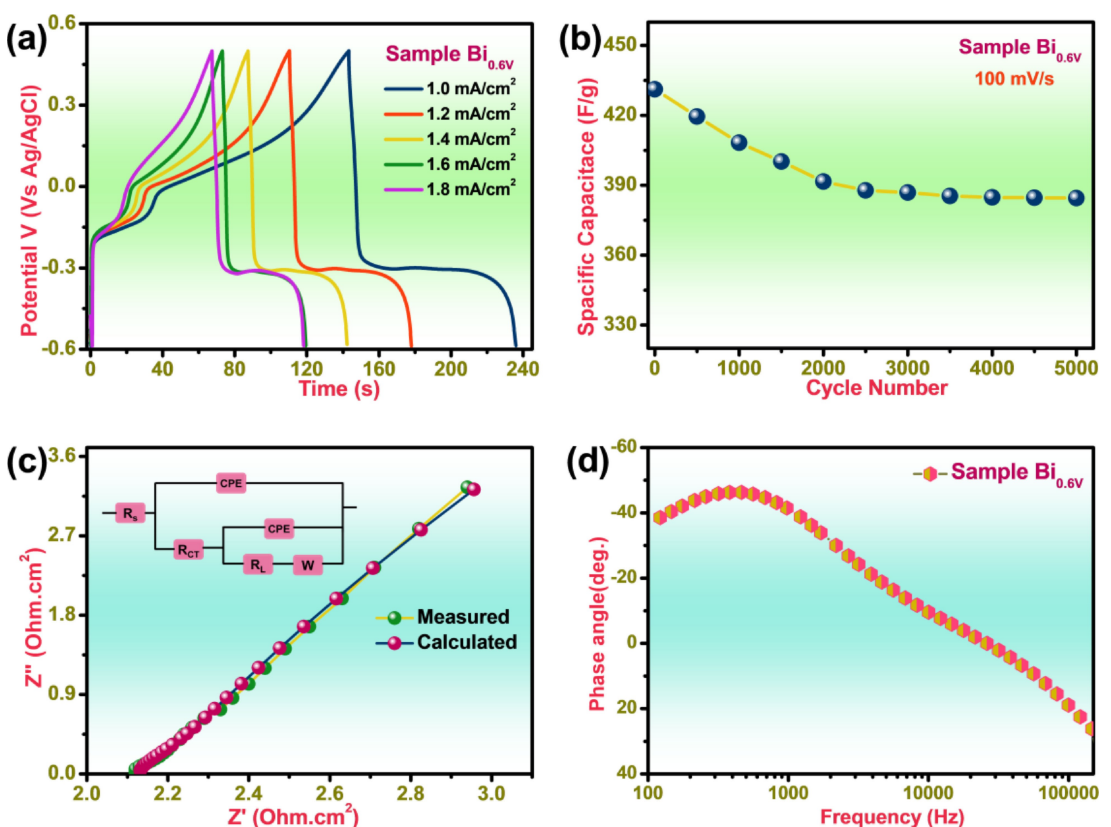


Figure 5. (a) chronopotentiometric curve of electrode Bi_{0.6V} at different current densities from 1.0 to 1.8 mA/cm², (b) stability plot study of Bi_{0.6V} electrode at constant 100 mV/s scan rate, electrochemical impedance spectroscopy of Bi_{0.6V} electrode (c) nyquist plot & matched nyquist plot, (d) bode plot.

behavior. As current density rises, the CP curve shifts in favor of symmetric behavior. The CP curve shows a reduction in potential drop, which implicates pseudocapacitive behavior. Due to supportive morphology and crystalline behavior, which provides the lowest diffusion lengths and quick transportation, good values of charging and discharging may be in the result. The stability plot of the Bi_{0.6V} electrode was shown in Figure 5 (b). It depicts the fluctuation of SC with cycle number in the potential window of 0.68 to 0.51 V vs. Ag/AgCl at 100 mV/s scan rate for 5000 cycles. The graph shows that the SC drops up to 3500 holding 138.3 F/g as the cycle number increases. Additionally, the Bi₂CuO₄ electrode exhibits consistent 137.6 F/g specific capacitance up to 5000 CV cycles as a cycle count rises. The extraordinary crystallinity and chemical durability of the Bi₂CuO₄ thin film electrode, where ionic transport is more rapid with smaller diffusion spans, are the causes of the stable specific capacitance. The drop in specific capacitance up to 3500 cycles may be caused by repeated electrolyte ion intercalation in the Bi₂CuO₄ matrix, suggesting that there may be a very minor deterioration of the substance.

EIS had been used to calculate an internal resistance of a Bi_{0.6V} electrode across the frequency extending from 1 mHz to 1 MHz in 1 M KOH electrolyte. Figure 5 (c) shows the real (Z') and imaginary (Z'') parts of a Nyquist impedance curve. Three primary areas may be seen on the Nyquist curve, including a miserable semi-circle at a greater frequency that is created by a similar arrangement of a charge transmission resistance (R_{CT}) carried on by a Faradaic process at a lesser frequency. Internal resistance (R_i) has been measured as

~2.1 Ω. A semi-circle's deviation, sometimes referred to as the knee frequency, indicates the highest frequency at which capacitive nature predominates. The Warburg resistance (Z_w) assessment, which depends on diffusion electrolyte ions resistance as per frequency, is shown by the portion of the curve with a 45° inclination and imaginary axis. Intercalation in electrode pores led to this outcome.^[23] The matched Nyquist graph of electrode Bi_{0.6V}. A Nyquist curve for electrode Bi_{0.6V} attained via experimentation and ordinary curve fit examined by ZsimpWin simulation software as in Figure 5 (c). An inset of Figure 5 (c) shows matched equivalent circuit for electrode Bi_{0.6V} have circuitry constraints viz charge transfer resistance R_{CT} = 1.812 Ω, R_{CT} = 32.22 Ω, R_L = 0.842 Ω, CPE = 9.94 × 10⁻⁹ F, CPE = 2.67 × 10⁻⁹ F, and W = 6.712 F. All the experiments were repeated numerous times and observed to be in decent agreement with enactment. Lower frequency behavior changing in the direction of the 'Y' axis reveals the electric double-layer capacitance (C_{dl}).

The Bode waveform for the Bi_{0.6V} electrode traced at OCP – 0.8594 V for 5 mA in 1 M KOH was displayed in Figure 5 (d). The Bode plot, representing the variation in phase angle with frequency, was an effective tool for comprehending the typical electrode characteristic. The corresponding phase angle in the relatively low-frequency range, as shown in Figure 5 (d), was significantly close to –40.1°, indicating that the constructed electrode was approximately supercapacitive (~–90°).^[31,33]

Asymmetric Device ($\text{Bi}_{0.6}\text{VII1 M PVA-KOH||AC}$) Performance

The three-electrode system's AC and $\text{Bi}_{0.6\text{V}}$ electrode CV curves were revealed in Figure 6 (a) at a scan rate of 100 mV/s. A plot displayed how well the AC and $\text{Bi}_{0.6\text{V}}$ electrodes operated as supercapacitors in the negative and positive potential windows of -1.4 to -0.6 V and -0.68 to 0.5 V against Ag/AgCl , correspondingly. Figure 6 (b) shows the CV graphs of the ASSD device ($\text{Bi}_{0.6\text{V}}\text{||1 M PVA-KOH||AC}$) scanned at various scan rates from 5 to 100 mV/s. The voltage span of the supercapacitor was optimized from -1.5 to 0.5 V . The curves closely resembled the rectangular type of CV, but due to the

presence of the pseudocapacitive positive electrode, tiny redox peaks were also seen. As revealed in Figure 6 (c), the SC was 73.7, 49.0, 42.2, 28.0, and 21.7 F/g at scan rates of 5, 10, 20, 50, and 100 mV/s, correspondingly. For practical usage, a supercapacitor could offer a broad working potential range. The graphs illustrated that as the scan rate increased, the integrated area also increased, indicating the optimal behavior of a capacitive device. The positive electrode's pseudocapacitive nature caused redox peaks to be seen. Peaks were also shown at scan speeds extending from 5 to 100 mV/s, suggesting that the supercapacitor had a quick redox response even at the advanced scan rates.

Figure 6 (d) showed a CP plot of the asymmetric supercapacitor device ($\text{Bi}_{0.6\text{V}}\text{||1 M PVA-KOH||AC}$) at various current densities. The

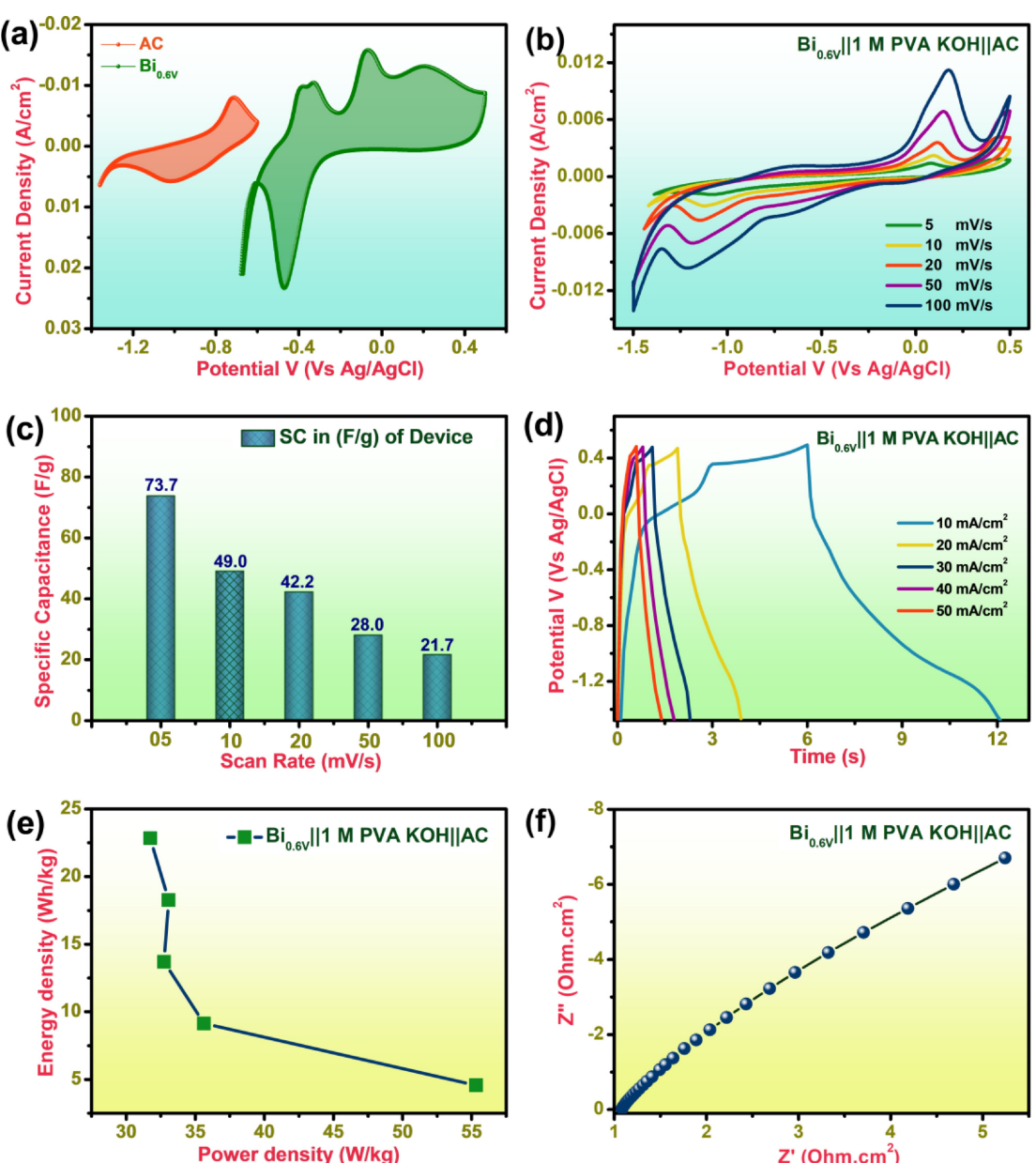


Figure 6. (a) CV curves of $\text{Bi}_{0.6\text{V}}$ electrode and AC electrodes at a scan rate of 100 mV/s, (b) CV curves of ASSD device ($\text{Bi}_{0.6\text{V}}\text{||1 M PVA-KOH||AC}$) at various scan rates from 5 to 100 mV/s, (c) specific capacitance in F/g of ASSD device ($\text{Bi}_{0.6\text{V}}\text{||1 M PVA-KOH||AC}$) Vs different scan rate, (d) chronopotentiometric curve of ASSD device ($\text{Bi}_{0.6\text{V}}\text{||1 M PVA-KOH||AC}$) at a different current density, (e) ragone plot of variation of energy and power density with specific current of ASSD device ($\text{Bi}_{0.6\text{V}}\text{||1 M PVA-KOH||AC}$), (f) Nyquist plot of ASSD device ($\text{Bi}_{0.6\text{V}}\text{||1 M PVA-KOH||AC}$).

supercapacitor's internal resistance and a linear capacitive discharge may have been responsibility for the discharging curve's rapid potential drop. At current densities of 10, 20, 30, 40, and 50 mA/cm², respectively, the energy and power densities were determined to be 55.3, 35.6, 32.8, 33.1, and 31.8 Wh/kg, and 4.6, 9.1, 13.7, 18.3, and 22.8 W/kg. The Ragone plot of the ASSD device ($\text{Bi}_{0.6}\text{v}||1\text{ M PVA-KOH||AC}$) fluctuated in SE and SP with the specific current in Figure 6 (e). Figure 6 (f) exhibited the electrochemical system (R_s) resistance of the asymmetric supercapacitor device ($\text{Bi}_{0.6}\text{v}||1\text{ M PVA-KOH||AC}$), which was modest due to the use of two highly conductive electrode materials. The internal resistance of the ($\text{Bi}_{0.6}\text{v}||1\text{ M PVA-KOH||AC}$) device was approximately 1.0 Ω . The Bode plot is a relation among the impedance phase angle and frequency as displayed in Figure S4. Interestingly, the plot of our ($\text{Bi}_{0.6}\text{v}||1\text{ M PVA-KOH||AC}$) device shows a phase angle value of -60.5° that is very close to -90° , approving impressive capacitance behaviour.^[31,33]

The SEM image after 5,000 cycles is shown in Figure S5 (a). After extended cycling, the material experienced significant changes, taking on a nearly spherical-like shape after initially having a structure like a spruce leaf. The post-stability images showed a deviation from the original leaf-like architecture, and while not perfectly spherical, they also reflected the initial structure. This morphological development illustrates the material's transformation and flexibility during extended use, suggesting dynamic structural changes taking place inside the material throughout the electro-

chemical cycling process.^[31,33] Figure S5 (b) shows the TEM images of electrode $\text{Bi}_{0.6}\text{v}$ after 5,000 cyclic stability studies. It reveals a consistent and well-defined plaquette-like (flake) structure. This distinct morphology suggests a robust and stable material, indicating its potential suitability for extended cycling and use in electrochemical applications.^[31,33] Additionally, as shown in Figure 7 (a) for long-term cycling performance, the asymmetric supercapacitor device ($\text{Bi}_{0.6}\text{v}||1\text{ M PVA-KOH||AC}$) could maintain 78.2% capacity for more than 5000 continuous CV cycles.

Given the typically low energy density of supercapacitors, which could limit their advanced applications, there was a pressing need to develop high-performance devices for use in modern electronics. At that time, the research direction revolved around enhancing the capabilities of supercapacitor technology by integrating ASSD devices from negative and positive electrodes with novel architectures. The construction of an asymmetrical device with a metal oxide-based cathode and a carbon-based anode was considered to potentially result in an extremely high energy density. Consequently, our proposed $\text{Bi}_{0.6}\text{v}$ electrode, which had demonstrated significantly better electronic properties through three-electrode analysis, was envisioned to serve as an outstanding cathode in the completed device. Meanwhile, the anode of the device was constructed with activated carbon, and 1 M PVA-KOH was chosen as a separator to be sandwiched between the two electrodes, as illustrated in Figure 7(b). Figure 7 (c) was an actual example of how an ASSD device ($\text{Bi}_{0.6}\text{v}||1\text{ M PVA-KOH||AC}$) lights a

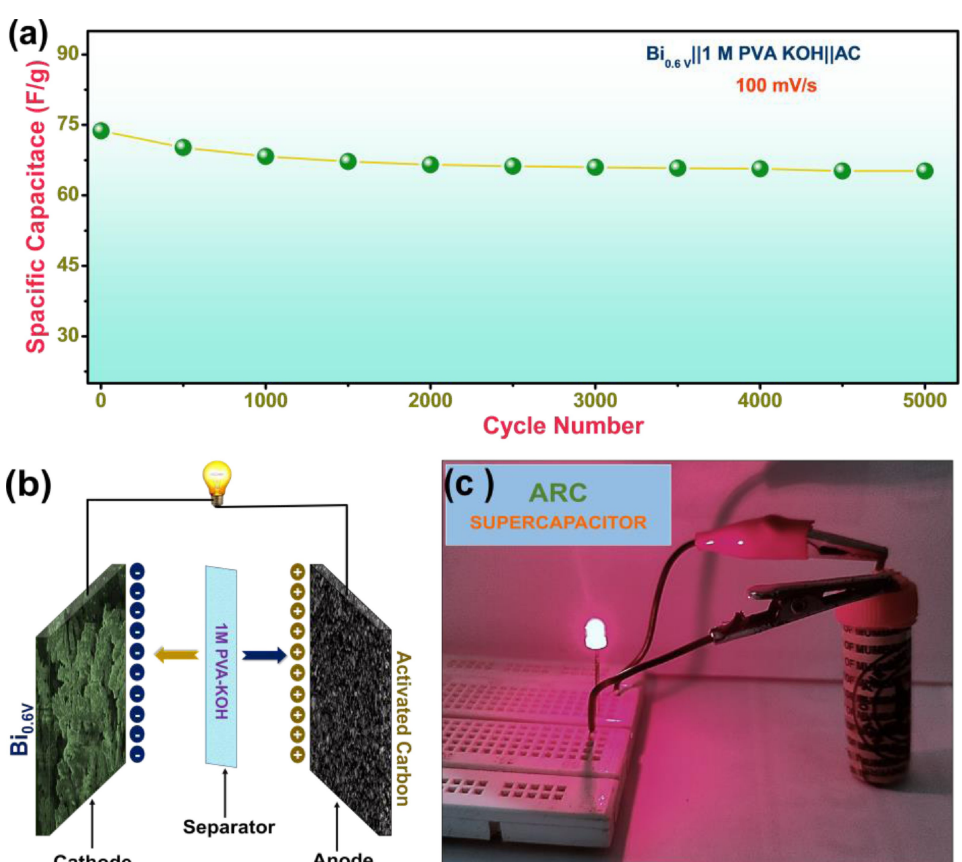


Figure 7. (a) stability plot study of ($\text{Bi}_{0.6}\text{v}||1\text{ M PVA-KOH||AC}$) device at constant 100 mV/s scan rate, (b) schematic representation showing the composition of ($\text{Bi}_{0.6}\text{v}||1\text{ M PVA-KOH||AC}$) device, (c) digital photographs of actual demonstration lighting the LED by using ($\text{Bi}_{0.6}\text{v}||1\text{ M PVA-KOH||AC}$) device.

red LED. An LED was discharged through a laboratory-scale asymmetric supercapacitor device ($\text{Bi}_{0.6}\text{Vl1 M PVA-KOHIIAC}$) to make it shine for 10–12 seconds after being charged by applying 2.0 V for almost 32 seconds.

Conclusions

In this work, a facile and simple electrodeposition route was revealed to synthesize Bi_2CuO_4 . Analyzing the crystal phases demonstrated that the annealed Bi_2CuO_4 electrode was in a tetragonal structure with a polycrystalline nature. The same exhibited a higher capacity of 431.2 F/g at 2 mV/s in 1 M KOH and 81.4% retention even at the end of 5000 continuous cyclic voltammetry cycles. Moreover, in the current work, Bi_2CuO_4 composites were developed as positive electrodes and AC as negative electrodes in the device fabrication. The capacity retention of the asymmetric supercapacitor solid-state device ($\text{Bi}_{0.6}\text{Vl1 M PVA-KOHIIAC}$) exhibited an excellent cyclic life of 78.2%. The ASSD ($\text{Bi}_{0.6}\text{Vl1 M PVA-KOHIIAC}$) device delivered a SE of 55.3 Wh/kg with an SP of 4570 W/kg. This research significantly resolved the problems of short-lived Bi_2CuO_4 thin film electrodes and poor electrochemical performance of metal oxide electrode materials for device construction.

Author Contributions

R. G. Bobade: Experimental synthesis, writing – original draft, Validation, Formal analysis, Software, and Visualization, S. F. Shaikh: writing – original draft, Validation, Formal analysis, editing, A. M. Al-Enizi: Validation, Formal analysis, Finishing, B. Pandit: Formal analysis, Editing, B. J. Lokhande: Supervision, editing & provide electrochemical characterization facility, R. C. Ambare: Supervision, Writing – review & editing-original draft.

Acknowledgements

Author Dr. Revanappa C. Ambare expresses gratitude to Prof. (Dr.) Balkrishna J. Lokhande for supplying the electrochemical characterization facilities. The authors extend their sincere appreciation to the Researchers Supporting Project number (RSP2024R55), King Saud University, Riyadh, Saudi Arabia for the financial support. Bidhan Pandit acknowledges the CONEX-Plus programme funded by Universidad Carlos III de Madrid (UC3M) and the European Commission through the Marie-Sklodowska Curie COFUND Action (Grant Agreement No. 801538). Bidhan Pandit also acknowledges Universidad Carlos III de Madrid (Agreement CRUE-Madroño 2024) for funding the article processing charge (APC) to make this article open access.

Conflict of Interests

The authors declare no conflict of interest.

Data Availability Statement

The data that support the findings of this study are available from the corresponding author upon reasonable request.

Keywords: Bi_2CuO_4 · Deposition Potential · Electrodeposition · Thin Film · Supercapacitor

- [1] F. Qi, H. Li, F. Yang, F. Sun, *Nanotechnology* **2021**, 32, 295705.
- [2] H. Li, F. Qi, F. Yang, Z. Sun, *J. Colloid Interface Sci.* **2021**, 587, 302–310.
- [3] X. Shi, *J. Power Sources* **2020**, 467, 228304.
- [4] R. C. Ambare, S. R. Bharadwaj, B. J. Lokhande, *Appl. Surf. Sci.* **2015**, 349, 887–896.
- [5] F. Qi, *J. Colloid Interface Sci.* **2021**, 601, 669–677.
- [6] H. Gobrecht, S. Seeck, H.-E. Bergt, A. Märtens, K. Kossmann, *Phys. Status Solidi* **1969**, 33, 599–606.
- [7] R. Irmawati, M. N. Noorfarizan Nasriah, Y. H. Taufiq-Yap, S. B. Abdul Hamid, *Catal. Today* **2004**, 93(95), 701–709.
- [8] U. T. Nakate, *Surfaces and Interfaces* **2019**, 17, 100339.
- [9] I.-I. Oprea, H. Hesse, K. Betzler, *Opt. Mater.* **2004**, 26, 235–237.
- [10] M. A. Abdelkareem, *Sci. Total Environ.* **2021**, 752, 141803.
- [11] S. S. Bhande, R. S. Mane, A. V. Ghule, S.-H. Han, *Scr. Mater.* **2011**, 65, 1081–1084.
- [12] C. Wang, *J. Colloid Interface Sci.* **2009**, 333, 242–248.
- [13] H. W. Kim, *Thin Solid Films* **2008**, 516, 3665–366.
- [14] Y.-W. Park, H.-J. Jung, S.-G. Yoon, *Sens. Actuators B* **2011**, 156, 709–714.
- [15] R. Chen, *J. Alloys Compd.* **2011**, 509, 2588–2596.
- [16] H. Xu, *Adv. Energy Mater.* **2015**, 5, 1401882, 1–7.
- [17] M. Gotić, S. Popović, S. Musić, *Mater. Lett.* **2007**, 61, 709–714.
- [18] S. Condurache-Bota, N. Tigau, A. P. Rambu, G. G. Rusu, G. I. Rusu, *Appl. Surf. Sci.* **2011**, 257, 10545–10550.
- [19] R. G. Bobade, *J. Mater. Sci. Mater. Electron.* **2024**, 35, 129.
- [20] T. P. Gujar, V. R. Shinde, C. D. Lokhande, S.-H. Han, *J. Power Sources* **2006**, 161, 1479–1485.
- [21] H. Su, *J. Appl. Electrochem.* **2014**, 44, 735–740.
- [22] N. Xia, *Mater. Res. Bull.* **2011**, 46, 687–691.
- [23] R. G. Bobade, *J. Energy Storage* **2024**, 84, 110776.
- [24] R. C. Ambare, S. V. Khavale, U. T. Nakate, M. B. Khanvilkar, B. J. Lokhande, *Colloids Surf. A* **2021**, 615, 126215.
- [25] K. S. Lee, Y. J. Seo, H. T. Jeong, *Carbon Lett.* **2021**, 31, 1041–1049.
- [26] A. Bera, *ACS Appl. Electron. Mater.* **2020**, 2, 177–185.
- [27] N. D. Nikolić, G. Branković, M. G. Pavlović, K. I. Popov, *J. Electroanal. Chem.* **2008**, 621, 13–21.
- [28] R. G. Bobade, *Inorg. Chem. Commun.* **2023**, 154, 110998.
- [29] P. J. Mafa, *J. Colloid Interface Sci.* **2021**, 603, 666–684.
- [30] C. Ren, *Adv. Funct. Mater.* **2020**, 30, 2004519, 1–14.
- [31] B. Pandit, *J. Energy Chem.* **2022**, 65, 116–126.
- [32] S. Anandan, G.-J. Lee, C.-K. Yang, M. Ashokkumar, J. J. Wu, *Chem. Eng. J.* **2012**, 183, 46–52.
- [33] B. Pandit, *IEEE Trans. Power Electron.* **2020**, 35, 11344–11351.

Manuscript received: March 6, 2024

Accepted manuscript online: March 12, 2024

Version of record online: April 24, 2024